GLOBAL BIOGEOCHEMICAL CYCLES, VOL. 10, NO. 1, PAGES 159–174, MARCH 1996

An atlas of the distribution of calcium carbonate in sediments of the deep sea

David E. Archer
Department of the Geophysical Sciences, University of Chicago

Abstract. Historical observations of the concentration of calcium carbonate in global deep sea sediments are compiled and compared with a new gridded field of seawater $CO_3^=$ concentration to reveal regional variations in the calcite lysocline. The most obvious mode of variability of the calcite lysocline is the thickness of the lysocline (defined here as the difference in overlying water carbonate saturation, $\Delta CO_3^=$, between high and low calcite sediments) with a thicker lysocline in the Atlantic than in the Pacific. I attribute this variation to differences in the delivery rate of terriginous material. A recent model for the lower glacial atmospheric pCO_2 proposed to change the relationship between the depth of the lysocline and the $\Delta CO_3^=$ of the water column by changing the rain rate ratio of organic carbon to calcite production (the "rain ratio model": Archer and Maier-Reimer, 1994). I search the data set for analogs to the proposed glacial world, by looking for a link between the regional climate at the sea surface and the depth of the lysocline below. The $\Delta CO_3^=$ at the carbonate compensation depth (CCD) in the tropics appears to be 10-20 $\mu mol\ kg^{-1}$ $\Delta CO_3^=$ more undersaturated than in high latitudes, but this is smaller than the ~40 $\mu mol\ kg^{-1}$ shift required by the model. In addition, the general resemblance of the glacial lysocline to the present day requires that the proposed shift in $\Delta CO_3^=$ at the CCD be globally uniform rather than locally variable, as climate forcing would probably generate. I conclude that the rain ratio model would probably require some globally uniform perturbation during glacial time, such as a change in ocean Si content, if it is to explain the entire pCO_2 decrease observed in the glacial atmosphere. Finally, I grid the sedimentary data to estimate that the inventory $CaCO_3$ which is available to neutralize fossil fuel CO_2 is approximately 1600 Gt carbon, a quantity which may be exceeded by fossil fuel release in the next several centuries.

Introduction

On time frames of thousands to hundreds of thousands of years, the CO_2 concentration in the atmosphere is controlled by processes that act in the ocean, and a central component of the ocean carbon cycle is the precipitation and burial of $CaCO_3$ in the deep sea. The budget for carbonate alkalinity in the ocean consists of addition from continental weathering, and removal by burial in shallow waters and in the deep sea. Burial of $CaCO_3$ in the deep sea occurs chiefly in sediments with high concentrations of $CaCO_3$, which are generally found in waters which are thermodynamically supersaturated or near saturation with respect to $CaCO_3$. The saturation state is controlled by the overlying water carbonate ion concentration ($[CO_3^=]$), and the pressure, with increasing solubility in deeper waters. Because of the pressure effect on calcite solubility, high-$CaCO_3$ sediments are found in shallow and intermediate depth waters, while sediments in the deepest waters are depleted with $CaCO_3$ (analogous to snow-capped mountains). An increase in ocean $[CO_3^=]$, such as would result from a deep sea burial rate insufficient to balance weathering minus shallow water burial, would tend to drive the "snow line" to greater depth, increasing the surface area of sediment where $CaCO_3$ is buried. Thus ocean $[CO_3^=]$ acts as a "homeostat" which on long enough timescales maintains steady state throughput of Ca^{2+} and $CO_3^=$ by making the deep sea burial rate a slave to the balance of weathering minus shallow water deposition [*Broecker and Takahashi,* 1978; *Berger,* 1982; *Keir and Berger,* 1985; *Broecker and Peng,* 1987; *Boyle,* 1988; *Opdyke and Walker,* 1992]. The significance of carbonate compensation to our understanding of climate is that ocean $CO_3^=$ to a large extent controls the pCO_2 of the atmosphere.

Significant progress has been made modeling the diagenesis of $CaCO_3$ in sediments, on diagenetic scales of centimeters [*Emerson and Bender,* 1981; *Keir,* 1982; *Archer et al.,* 1989; *Hales et al.,* 1993], basin "lysocline" scales [*Emerson and Archer,* 1990; *Archer,* 1991a], and global scales [*Keir,* 1990; *Emerson and Archer,* 1992; *Archer and Maier-Reimer,* 1994]. The models have reached the point where subtleties of the carbonate distribution on the seafloor might be interpretable or serve to differentiate between model formulations and assumptions. One goal of this paper is to digest available sedimentary data into a format suitable for validating models of $CaCO_3$ dynamics in the ocean.

A second goal is to estimate the inventory of deep sea $CaCO_3$ which will be available for neutralization of fossil fuel CO_2. Carbonate dissolution in deep sea sediments is thought

Paper number 95GB03016.
0886-6236/96/95GB-03016$10.00

to occur mostly within the top few centimeters of the sediment column, which is within the bioturbated layer of the sediment. According to diagenetic models of carbonate dissolution, when the bioturbated layer becomes filled with noncarbonate sediments such as terriginous clay materials, dissolution effectively ceases. Therefore for a dissolution response, the extent of neutralization may be limited by the availability of deep sea carbonates [*Broecker and Takahashi,* 1978].

A third specific target is to address a question stimulated by recent modeling results. The question is: How variable is the preservation of $CaCO_3$ relative to local saturation conditions? A recent coupled sediment / water column carbon cycle model predicted that the pH of the ocean, and the pCO_2 of the atmosphere, ought to be sensitive to the relative rain rates of organic carbon and calcium carbonate that reach the seafloor [*Archer and Maier-Reimer,* 1994]. The model proposes to move the calcite lysocline relative to the saturation state of the overlying water by changing the ecosystem dynamics (and the resulting balance between organic carbon and calcium carbonate production rates) at the sea surface. In this paper I examine the link between climate at the sea surface and the preservation of $CaCO_3$ below. In effect, I am searching for an analog for the glacial world proposed by the rain ratio model. If the shift in climate between glacial and today was sufficient to drive a shift in production which in turn drove a change in the preservation of $CaCO_3$, then perhaps regional climate variation in today's world will also leave a signature in the lysocline below.

To address these questions, I compiled and gridded a global data set of the dry weight percent of calcium carbonate in deep sea coretop sediments, and generated a gridded field of the water column carbonate chemistry. The gridded $\Delta CO_3^=$ field in the water column enabled me to extract a $\Delta CO_3^=$ value for the overlying water corresponding to each $\%CaCO_3$ observation in the $\%CaCO_3$ data set. The gridded $\%CaCO_3$ field on the seafloor facilitates comparison with gridded predictive models, such as the *Archer and Maier-Reimer* [1994] model, and allows calculation of the global inventory of sediment surface $CaCO_3$ (which will eventually neutralize fossil fuel CO_2 [*Broecker and Takahashi,* 1978]).

Distribution Patterns of $CaCO_3$ in Deep Sea Sediments

The well-known relationship between water depth and sedimentary $CaCO_3$ concentration in the deep sea is caused by the effect of pressure on calcite solubility. This relationship is complicated, however, by the acidification of the deep sea by respiration of organic debris settling from above. Because of this effect, the Atlantic, with recently ventilated high pH deep water, preserves carbonates in deeper waters than does the Pacific, where deep water has been acidified by respiration. In order to more simply interpret the sedimentary $\%CaCO_3$ data, we would like to examine the distribution of $CaCO_3$ relative to the saturation state for calcite, $\Delta CO_3^=$, rather than relative to water depth. $\Delta CO_3^=$ ought to serve as a "normalized" vertical coordinate, such that the lysocline from the Atlantic and the Pacific can be directly compared.

Sedimentary Data

Historical data for the distribution of calcium carbonate in coretop sediments was compiled from the literature. The data was presented by *Biscaye et al.* [1976], *Berger et al.* [1976], *Cweink* [1986], and *Kolla et al.* [1976]. Much of the data originated in the Scripps Sedimentological data set, compiled by Gustaf Arhenius and colleagues. The reconstructed data set consists of nearly 3800 $\%CaCO_3$ data points, consisting of a core ID, location, depth, and dry weight percent $CaCO_3$. The data are generally from what are visually observed to be the tops of retrieved sediment cores; however some data points may actually represent older sediment than late Holocene, due to the difficulty of retrieving intact near-surface sediment, or to slow accumulation of sediment in some regions. The locations and coverage of the $\%CaCO_3$ data are shown in Figure 1.

Gridded GEOSECS [$CO_3^=$]

A global data set of water chemistry measurements is available in the GEOSECS data [*Takahashi et al.,* 1980], but the locations of water chemistry observations are seldom the same as the locations of sedimentary data. Therefore it was necessary to extrapolate the GEOSECS carbonate data to a

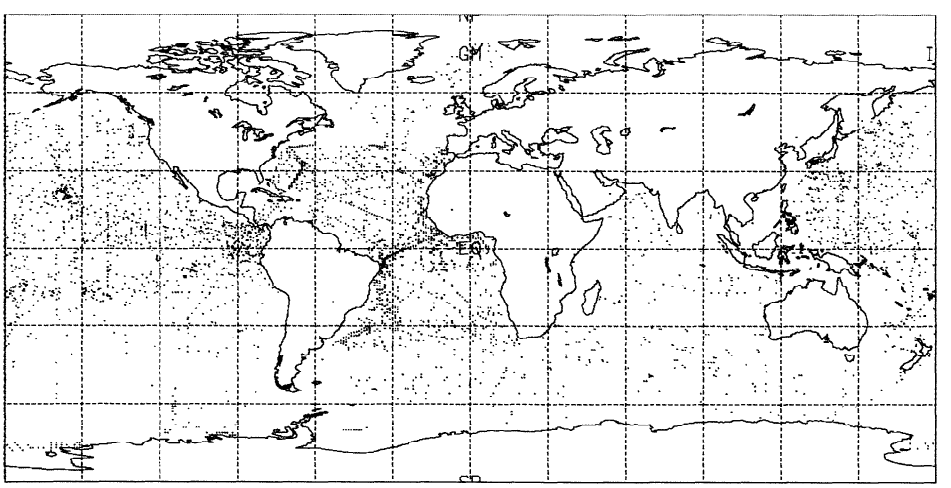

Figure 1. Map of the locations of coretop $\%CaCO_3$ measurements.

Tables

Table 1. Coefficients Used to Predict Water Column $[CO_3]$

Independent Variable	Coefficient	Sample Value	Contribution
Constant	-103.75		-103.75
Depth, m	-1.7761E-3	1750	-3.10
$Sigma_0$	0.237173	27.191	6.44
$Sigma_0^2$	0.213864	739.73	158.20
$K_{h\ CO2}$	1.307094	54.37	71.06
T, C	9.001017	3.84	34.56
Sal, PSU	-2.877497	34.98	-100.65
O_2, μM	0.272188	241.62	65.76
PO_4, μM	-20.42355	1.21	-24.71
SiO_4, μM	0.283039	18.19	5.14
Latitude, deg	3.4131E-2	-1.5	-0.05

"Typical Value" and "Contribution" columns are used to illustrate the method. We are able to predict GEOSECS CO_3 values, using the independent variables listed, with rms sigma = 10.5 μM. Much of the error occurred at the sea surface; when data from the to 500 m were eliminated, the rms sigma = 7.8 μM.

global domain. Rather than simply linearly extrapolate data in space, our extrapolation is based on an empirical relationship between $CO_3^=$ and T, S, O_2, and nutrient data from GEOSECS, and gridded data sets of T, S, O_2, and nutrient data from *Levitus* [1982] and *Levitus et al.* [1993]. Water column $[CO_3^=]$ was calculated from GEOSECS alkalinity, total CO_2, temperature, salinity, nutrient, and pressure data, using the carbonic acid dissociation constants of *Mehrbach et al.* [1973] with pressure dependence of *Culberson and Pytkowicz* [1968], and borate dissociation constants of *Lyman* [1956]. Although more recent dissociation constants are available [*Dickson and Millero,* 1987], the historical constants were used in order to be consistent with calcite solubility formulation of *Sayles* [1980], which was used to calculate $\Delta CO_3^=$.

Within the GEOSECS data set, an empirical relationship was derived relating $[CO_3^=]$ to other elements of the data set using a multiple linear regression technique. The relationship takes the form

$$[CO_3^=] = \Sigma_i A_i \times P_i$$

where A_i are the calculated least square coefficients and P_i are other measurements that might co-vary with $CO_3^=$, such as T, S, $[O_2]$, $[SiO_2]$, etc. Sets of coefficients A_i were calculated for a variety of combinations of data, and the best fit to the data was found using the combination of A_i and P_i listed in Table 1.

The gridded sea water $[CO_3^=]$ field was generated based on the empirical coefficients A_i from the GEOSECS data and the gridded fields of P_i (T, S, $[NO_3^-]$, etc.) from *Levitus* [1982] and *Levitus et al.* [1993]. The Levitus et al. data sets were compiled using an "objective mapping" of historical data archived at the National Oceanographic Data Center, and represent the best existing pictures of the physical and chemical structure of the water column. The resulting gridded $CO_3^=$ data set has the same resolution as that of the Levitus et al. fields: 1° square by 33 depths. The analysis was tested by extracting values from the gridded $[CO_3^=]$ field corresponding to the locations of GEOSECS data, and comparing them with the GEOSECS measurements. We find that the optimal relationship (Table 1) gives an rms deviation between GEOSECS and gridded $[CO_3^=]$ data of 10.5 μmol kg^{-1}. However, the fit is better in the deep ocean; rms deviation = 7.8 μmol kg^{-1} $CO_3^=$ for the values below 500 m depth. This uncertainty approaches the analytical variability of the calculated $[CO_3^=]$ in the original data set.

Profiles of $\Delta CO_3^=$ values predicted by the method are compared with GEOSECS data in Figure 2, and sections of $\Delta CO_3^=$ are given in Figure 3. Contour plots of the depths of various constant $\Delta CO_3^=$ surfaces (such as saturation horizon, where $\Delta CO_3^= = 0$) are given in Figure 4. The apparent sharp front in the depth of the saturation horizon in Figure 4 is the result of the undersaturation of intermediate water; the $\Delta CO_3^= = 0$ surface actually folds under itself in the North Pacific. The $\Delta CO_3^=$ at the sediment surface is given in Figure 5. To generate this field, the $CO_3^=$ concentration from the deepest cell in the gridded field was compared with $CaCO_3$ solubility at the depth of the sea floor based on a gridded field of ocean bathymetry (ETOPO 5, available from the National Geophysical and Solar Terrestrial Data Center of the National Oceanographic and Atmospheric Administration). An estimate of the overlying water saturation state above each sediment $\%CaCO_3$ observation was calculated in a similar way, adding a fourth coordinate, the $\Delta CO_3^=$ of the overlying water, to the latitude, longitude, and depth coordinates of the ungridded $\%CaCO_3$ data set.

Results

The $\%CaCO_3$ versus $\Delta CO_3^=$ data are split into Atlantic and Pacific/Indian and plotted in Figure 6. The decrease of $CaCO_3$ with $\Delta CO_3^=$ can be seen in both plots. Histograms on the left

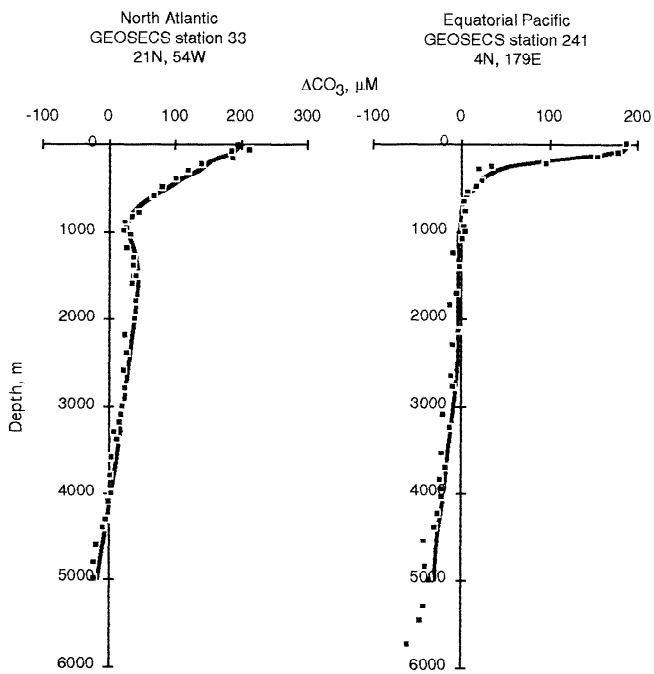

Figure 2. Comparison of regression-predicted $\Delta CO_3^=$ profiles with data from GEOSECS.

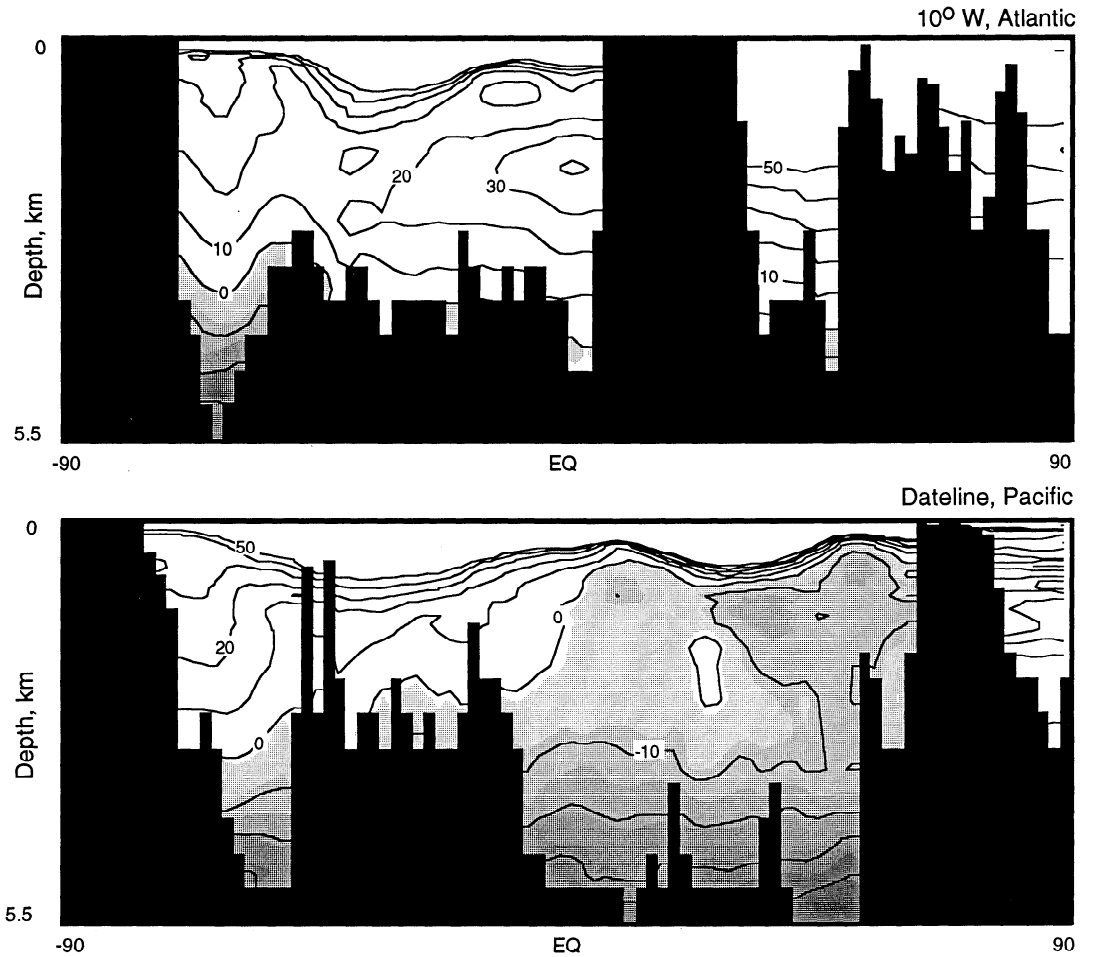

Figure 3. Sections of $\Delta CO_3^=$ from Atlantic and Pacific oceans. Units are micromoles per kilogram.

sides of the plots show the number of observations as a function of $\Delta CO_3^=$. As noted above, the water overlying the seafloor has generally higher $\Delta CO_3^=$ (more saturated) in the Atlantic than in the Pacific / Indian oceans. This factor alone tends to bias the data clouds in the Pacific / Indian oceans to the lower parts of the plots. However, the Pacific / Indian data do not appear to be simply a subsample of the wider range of $\Delta CO_3^=$ spread in the Atlantic; the transition to high $CaCO_3$ sediments seems to occur at a significantly lower $\Delta CO_3^=$ in the Pacific / Indian. The average $\%CaCO_3$ is $10 \pm 2\%$ higher within a range of -20 to -25 μmol kg^{-1} $\Delta CO_3^=$ in the Indian / Pacific than in the Atlantic, where the uncertainty is the standard error of the mean.

To explore the observation of a systematic difference between Atlantic and Pacific/Indian $\%CaCO_3$ distributions, the data are resolved spatially into "tiled" plots of the lysocline in Figures 7a and 7b. Global maps of the Earth's surface have been superimposed with a grid which divides the earth into 20° × 20° squares. Inside each square in the grid is a plot of the calcite lysocline using data which originate somewhere in the region of the map covered by the square. In Figure 7a the vertical ordinate of each plot is depth (ranging from 0 to 6000 m), with $\%CaCO_3$ ranging from 0 to 100% on the horizontal axis. Figure 7b is similar to Figure 7a except that each vertical axis is $\Delta CO_3^=$, on a scale of +50 μM at the top to -50 μM at the bottom. Dashed lines indicate the $\Delta CO_3^= = 0$ saturation horizon in Figure 7b. Thus, each square on the maps represents one regional plot of the calcite lysocline, and the lysocline plots are tiled together like a sheet of stamps to show the areal distribution of the shape of the lysocline and the coverage of available data.

As discussed above, the $\%CaCO_3$ / depth relation (Figure 7a) contains within it variations in the pH of the deep water of the ocean, while plots of $\%CaCO_3$ as a function of $\Delta CO_3^=$ (Figure 7b) represent the more dynamically revealing picture of the calcite distribution. Several features are immediately evident from Figure 7b. First, the lysocline is "cleanest" in tropical and subtropical pelagic sediments; in contrast, in near-coastal sediments, and in the Southern Ocean, the distribution of $\%CaCO_3$ shows more scatter and less clear dependence on depth. Second, in those regions where the calcite concentration appears to be simply controlled by $\Delta CO_3^=$, the "thickness" of the transition zone (lysocline) is much greater in the Atlantic than it is in the eastern Pacific Ocean. Finally, we note that the carbonate compensation depth (CCD) is found at higher degrees of undersaturation in the central equatorial

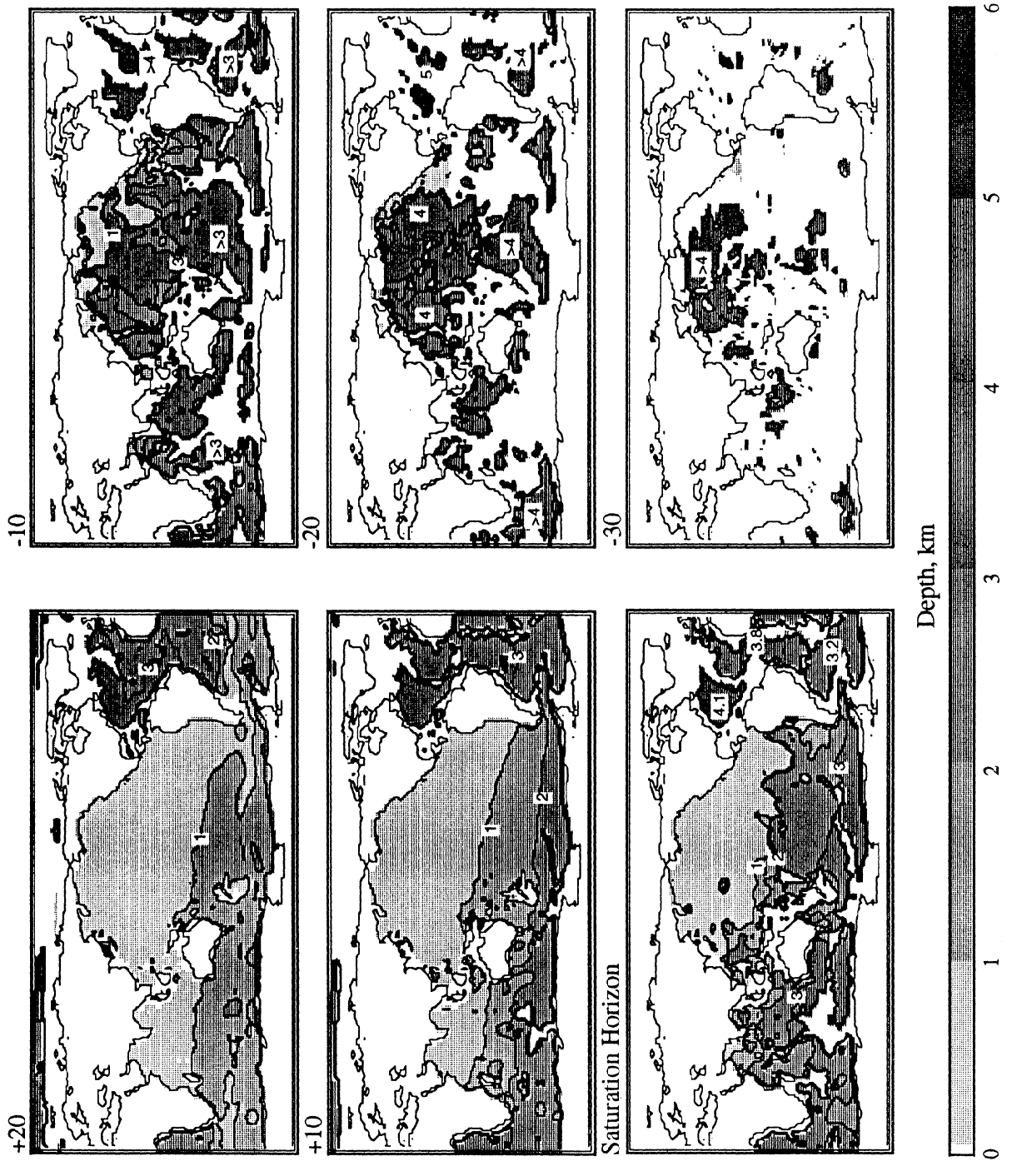

Figure 4. Depth of various constant $\Delta CO_3^=$ surfaces, such as the saturation horizon where $\Delta CO_3^= = 0$, in kilometers. The sharp front in the depth of saturation in the North Pacific is due to a "shelf" of undersaturated intermediate water ; the $\Delta CO_3^= = 0$ surface actually folds under itself in this region.

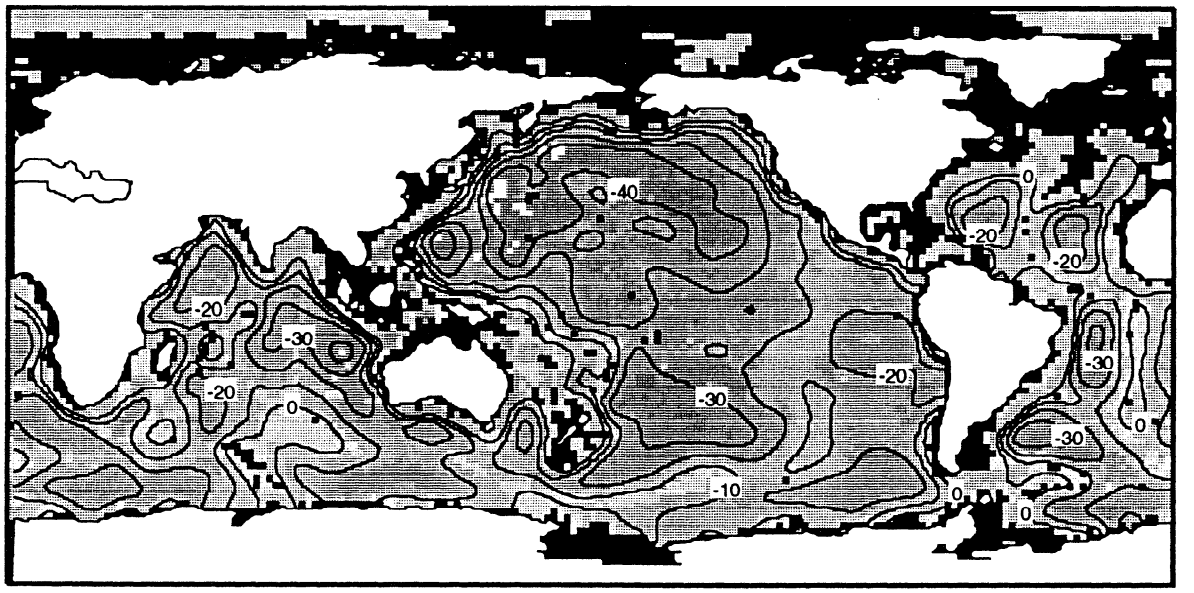

Figure 5. $\Delta CO_3^=$ at sediment surface, obtained by extrapolating the water column $CO_3^=$ to the depth of the sediment, and calculating calcite solubility at that depth.

Pacific; that the depth of the CCD is shallower in all directions from this location. These observations will emerge more clearly with further analysis below.

Regional variation in the thickness of the transition zone. In order to quantify the regional variability of the shape of the lysocline, I calculate two diagnostic parameters from each 20° × 20° region using methodology of *Archer* [1991a]. One parameter is the "thickness" of the lysocline, called T_{lys}, which is the range in $\Delta CO_3^=$ which is required to drive the sediments from high $CaCO_3$ values to zero $CaCO_3$: the slope of the $\%CaCO_3$ vs. $\Delta CO_3^=$ relation within the lysocline. The other is the $\Delta CO_3^=$ at the CCD, called ΔCO_3^{CCD}, which can be viewed as the zero intercept of the $\%CaCO_3$ vs. $\Delta CO_3^=$ relation. *Archer* [1991a] found that model lysocline dependence on organic carbon, $CaCO_3$, and dilutant material rain rates could be conveniently expressed in terms of T_{lys} and ΔCO_3^{CCD}.

Values for T_{lys} and ΔCO_3^{CCD} for data within each suitable 20° × 20° square region were calculated by linear regression of $\%CaCO_3$ versus $\Delta CO_3^=$ (Table 2). Regions where the $\Delta CO_3^=$ dependence of $\%CaCO_3$ was unclear, such as continental margins, were excluded (by hand selection) from the calculation. Within each region, data points with $\%CaCO_3$ lower than 5% or higher than 70% were excluded as potentially being outside the region of $\%CaCO_3$ dependence on $\Delta CO_3^=$ (the lysocline). The data were then fit to an equation of the form

$$\%CaCO_3 = A \times \Delta CO_3^= + B \qquad (1)$$

T_{lys}, in units of μmol kg^{-1} $CO_3^=$, was calculated as

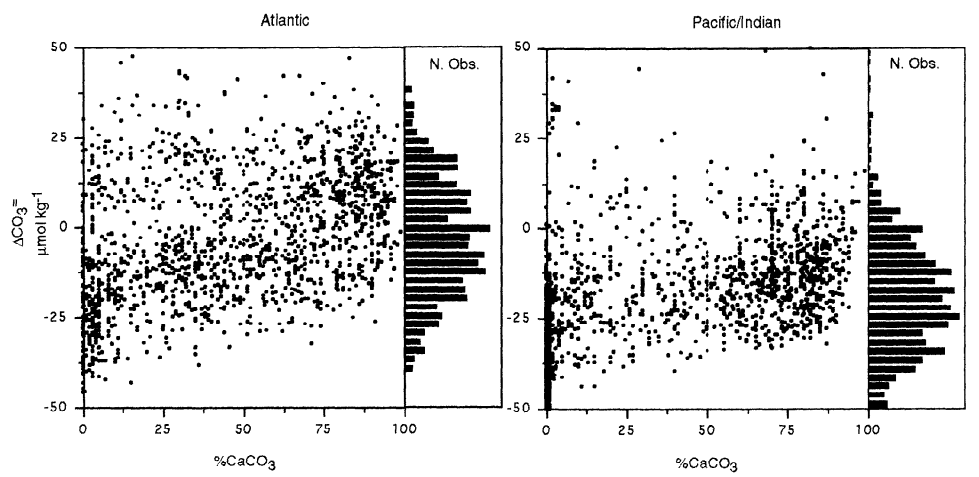

Figure 6. $\%CaCO_3$ data plotted as a function of the overlying water $\Delta CO_3^=$, for the Atlantic and Pacific/Indian oceans. Histograms on the right sides of the plots show the distribution of observations.

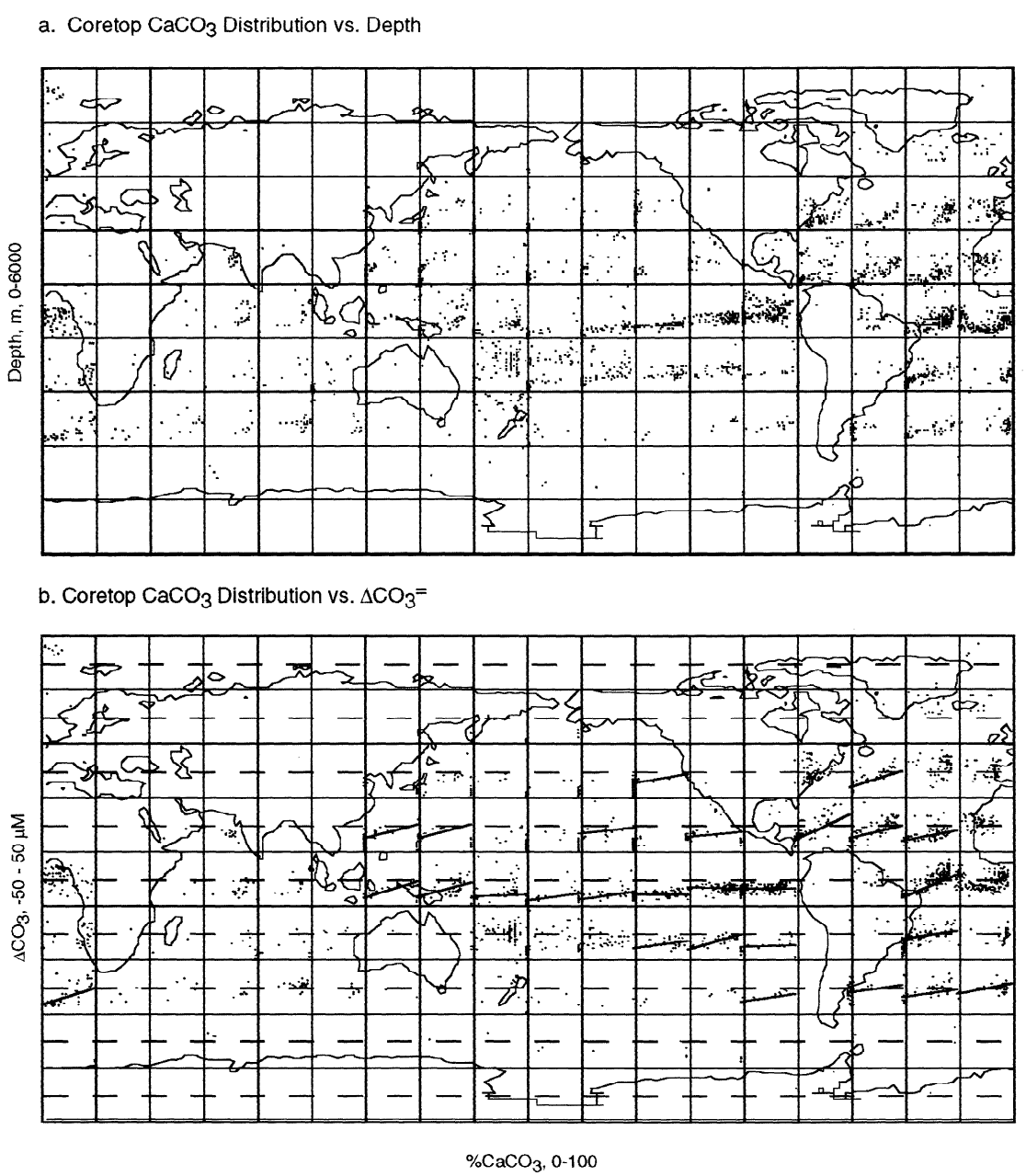

Figure 7. Tiled plots of the lysocline, in vertical space of (a) depth, 0-6000 m and (b) ΔCO_3, -50 - 50 micromoles per kilogram. See text for explanation.

$$T_{lys} = [CO_3^{=}]_{(\%CaCO_3=80\%)} - [CO_3]_{(\%CaCO_3=0)} \qquad (2)$$

The other diagnostic is the degree of undersaturation at the CCD,

$$\Delta CO_3^{CCD} = \Delta CO_3^{=} (\%CaCO3 = 0) = -B/A \qquad (3)$$

also in units of μmol kg^{-1} $CO_3^{=}$. Regression lines based on the calculated values of T_{lys} and ΔCO_3^{CCD} are shown plotted on top of the data in Figure 7b.

Values of T_{lys} calculated from the regression lines in Figure 7b are plotted against their corresponding values of ΔCO_3^{CCD} in Figure 8a. The observations are grouped in three classifications; equatorial, tropical, and subtropical, represented by diamonds, circles, and squares, respectively. The full range of variability in both parameters appears to be covered by all three provinces. While a full numerical analysis of the data is beyond the scope of this paper, two lines of evidence suggest that the observed patterns of T_{lys} and ΔCO_3^{CCD} are caused by variations in the rate of dilution by

Table 2. Values of ΔCO_3^{CCD}, T_{lys}, and Number of Observations for Various Ocean Areas

Latitude	Longitude	Number of Obs.	ΔCO_3^{CCD}	T_{lys}
40	150	7	-42	43
40	230	10	-18	17
40	310	29	-27	29
20	130	7	-23	26
20	150	12	-22	27
20	210	15	-14	14
20	250	15	-19	9
20	290	47	-24	46
20	310	31	-21	23
20	330	46	-28	20
0	130	8	-34	32
0	150	18	-31	26
0	170	12	-30	4
0	190	9	-38	13
0	210	18	-35	13
0	230	44	-28	0
0	250	50	-14	-1
0	270	113	-16	0
0	330	71	-34	44
-20	110	6	-25	21
-20	230	10	-25	13
-20	250	34	-30	28
-20	270	8	-24	3
-20	330	54	-10	15
-40	10	31	-34	33
-40	90	7	-6	15
-40	270	5	-26	14
-40	310	11	-10	16
-40	330	17	-19	16
-40	350	6	-13	21

Longitude and Latitude are given for the center of a given 20 x 20 degree box.

non-$CaCO_3$ material. First, the model-predicted signature of dilution on the steady state shape of the lysocline is to increase T_{lys} while maintaining roughly constant ΔCO_3^{CCD}, as observed in the data (Figure 8b) [*Archer*, 1991a]. There is also a general trend toward "thicker" lysoclines in regions where higher dust flux to the oceans is expected: the Atlantic and to the east of Asia [*Duce et al.*, 1991]. In Figure 8a, the T_{lys} versus ΔCO_3^{CCD} observations are divided into classifications "eastern" and "western", where a location is defined as "western" if it is located within 60 degrees of a continent to the west, and "eastern" otherwise (the only part of the world's ocean that qualifies for an "eastern" classification is the eastern Pacific). Eastern data locations are filled, while points from western regions are open. Western lysoclines clearly tend to have higher values of T_{lys} than eastern lysoclines. Thus proximity of the sediment to the western edge of the basin appears to be a stronger determinant of T_{lys} than is latitude.

Latitudinal variation in the $\Delta CO_3^=$ of the CCD. As explained in the introduction, we are interested to see if the climate and corresponding plankton ecosystem structure at the sea surface has any clear signal in the $CaCO_3$ concentration in the sediments below. The primary indicator of marine climate is latitude, so we examine plots of $\%CaCO_3$ versus latitude at constant $\Delta CO_3^=$ (±2.5 μmol kg^{-1}), to see the effect of latitude on $CaCO_3$ preservation in Figure 9. At $\Delta CO_3^=$ of -10 μmol kg^{-1} or lower, $CaCO_3$ is completely depleted in sediments in middle and high latitudes. In contrast, some low latitude locations contain high $CaCO_3$ with overlying water $\Delta CO_3^=$ as low as -30 μmol kg^{-1}. Thus it appears that tropical sediments may tend to preserve $CaCO_3$ deeper in the water column than middle and high-latitude sediments.

The longitudinal extent of this "anomalous tropical preservation" is resolved in Figure 10. At each value of $\Delta CO_3^=$, the $\%CaCO_3$ observations are interpolated onto a continuous gridded surface of latitude and longitude using a weighted averaging technique. Each gridded surface is shown only where water at that value of $\Delta CO_3^=$ exists. The resulting figures are analogous to isopycnal concentrations of nutrients, for example, with $\Delta CO_3^=$ in place of density and $\%CaCO_3$ in place of nutrients. Since $\%CaCO_3$ is not a property of the water column but rather of the sediments, the $\%CaCO_3$ field

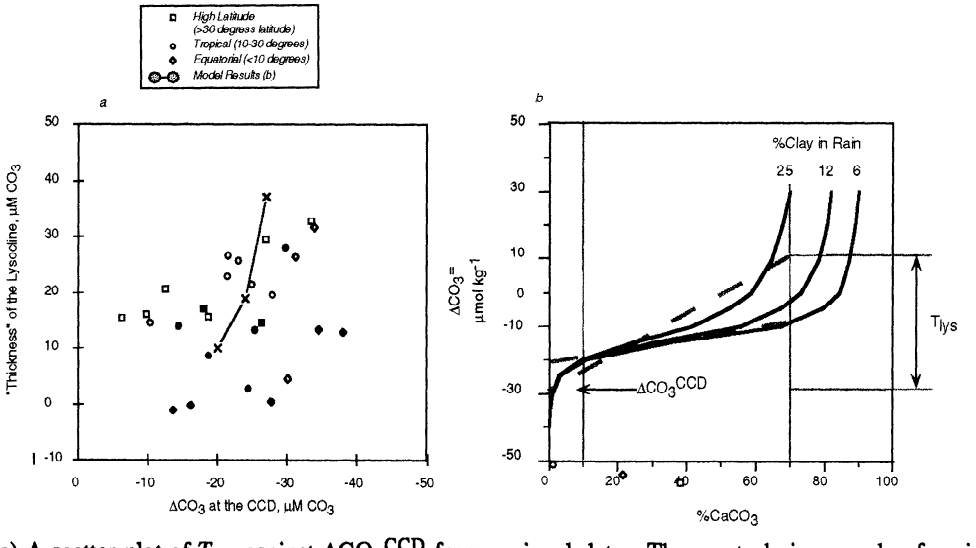

Figure 8. (a) A scatter plot of T_{lys} against ΔCO_3^{CCD} from regional data. The most obvious mode of variability of the lysocline is variation in lysocline thickness, with thicker lysoclines in the western parts of ocean basins, where fluxes of atmospheric dust are higher. (b) Model results showing that dilution of calcite tends to increase lysocline thickness (T_{lys}), while maintaining nearly constant penetration (ΔCO_3^{CCD}).

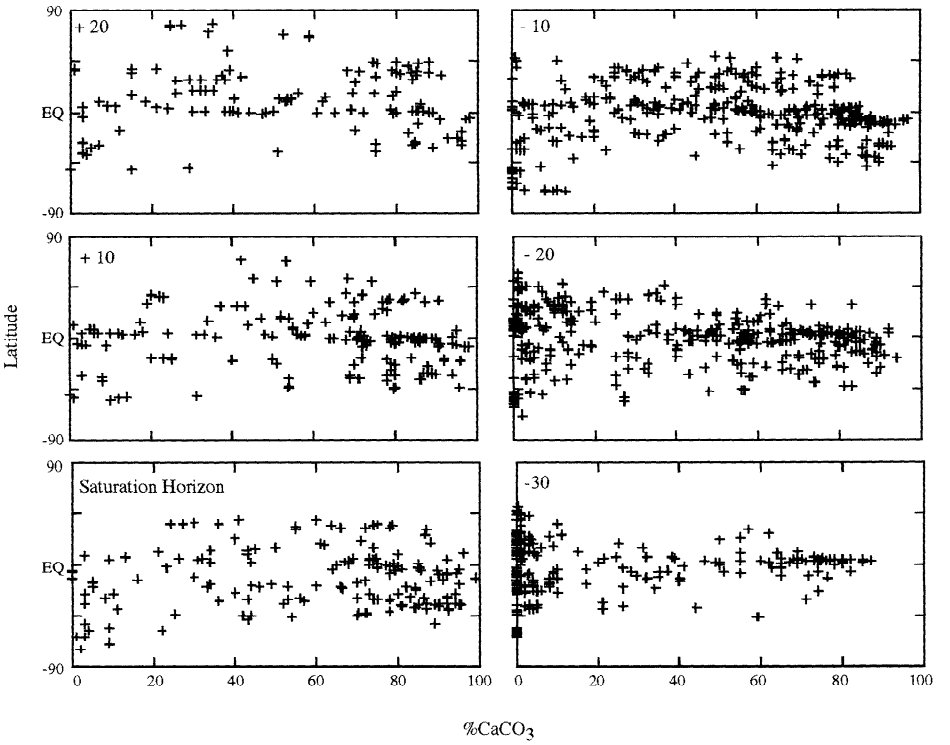

Figure 9. Scatter plots of $\%CaCO_3$ filtered by overlying water ΔCO_3 (micromoles per kilogram) and plotted as a function of latitude. Calcite tends to be preserved under more corrosive conditions in tropical sediments.

represents expected values in any sediments that happen to be located in this $\Delta CO_3^=$ surface at a given latitude and longitude. The maps were generated by a weighted interpolation technique. Each data point was assigned a "crowding coefficient" equal to the sum of the inverses of distances of other sedimentary observations, as

$$C_i = \sum_j \left(\frac{1}{R_{ij}} \right) \tag{4}$$

where i is a data location, j is the series of nearby data locations, and R_{ij} is the distance from the data location i to data location j. Observations that are closely spaced have higher values of this coefficient. Construction of a gridded field of $\%CaCO_3$ was based on a weighted averaging scheme, where the influence of the value of an observation on the value of the interpolated field scales with proximity (inversely with R_{ij}), and inversely with the "crowding coefficient" of the observations, as

$$\%CaCO_{3_f} = \frac{\sum_i \%CaCO_{3_i} R_{if}^{-1} C_i^{-1}}{\sum_i R_{if}^{-1} C_i^{-1}} \tag{5}$$

where the point f is the target "field" value, and the points i are the input data values. The crowding scheme helps eliminate an artifact of duplicate or near-duplicate data dominating the output field simply by "strength in numbers".

Much of the calcite observed at $\Delta CO_3^=$ = -30 μmol kg^{-1} in Figure 10 comes from the equatorial Pacific, a region which may potentially be out of steady state following the glacial termination [*Farrell and Prell,* 1989; *Berelson et al.,* 1994]. Of the eight observations of ΔCO_3^{CCD} at $\Delta CO_3^=$ equals -30 μmol kg^{-1} or lower, five are located in the western or central equatorial Pacific, one in the equatorial Atlantic, and two in the subtropical regions. If the low $\Delta CO_3^=$ of the CCD is caused by nonsteady state behavior, then its isolation to the equator must indicate a change in equatorial production rather than water column chemistry, implying that during glacial time there was an enhancement of $CaCO_3$ burial at the equator. The alternative possibility is that the equatorial anomaly is caused by a present day productivity gradient. Either way, the picture of enhanced preservation in low latitudes (the equatorial region in particular) appears to persist. The gradient between high calcite preservation in high latitudes (which can be seen at $\Delta CO_3^=$ = -10 μmol kg^{-1}) and low latitudes (- 30 μmol kg^{-1}) points to a "tropical calcite preservation enhancement" of order 10 - 20 μmol kg^{-1} $CO_3^=$.

Implications for the rain ratio model. A central goal of this project was to evaluate the "rain ratio model" for generating low glacial pCO_2 [*Archer and Maier-Reimer,* 1994]. The model was based on an ocean circulation / carbon cycle model [*Maier-Reimer,* 1993] coupled to a mechanistic model of $CaCO_3$ dissolution in sediments [*Archer,* 1991a]. Alkalinity and dissolved CO_2 were added to the surface ocean at a rate designed to simulate the effect of terrestrial chemical weathering. The global removal rate of $CaCO_3$ was determined by the rain rate of $CaCO_3$ to the seafloor, predicted by the ocean model, and the rate of $CaCO_3$ dissolution, predicted by the sediment model. The $[CO_3^=]$ of the model ocean was

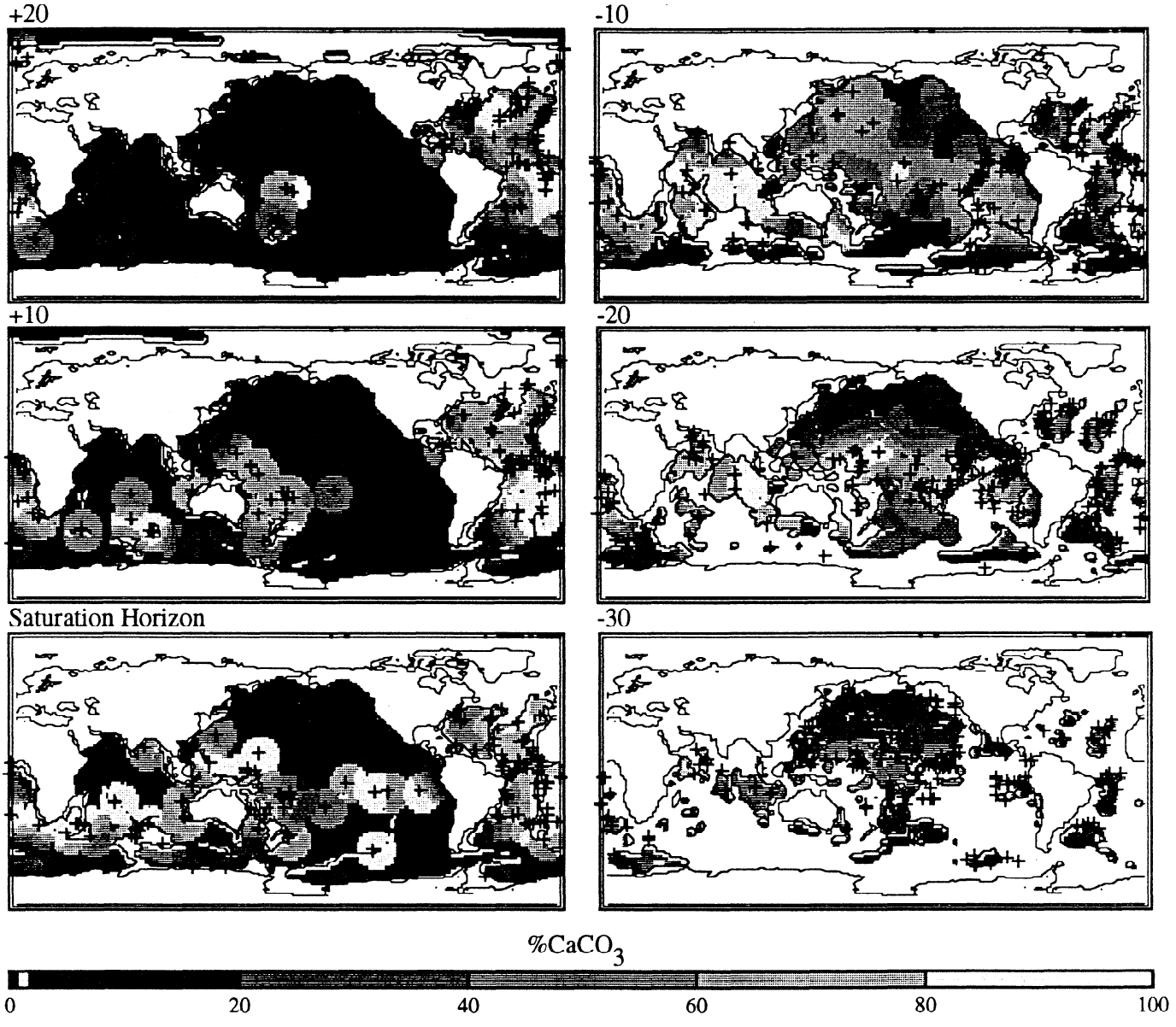

Figure 10. Maps of $\%CaCO_3$ observations filtered by overlying water $\Delta CO_3^=$ (micromoles per kilogram). Calcite tends to be preserved under slightly more corrosive conditions in tropical sediments.

allowed to float until it found the value at which burial of $CaCO_3$ in the deep sea balanced the weathering influx of alkalinity and total CO_2. In this way the model was able to simulate $CaCO_3$ compensation in the ocean.

The novel aspect of this model formulation was that the sediment dissolution model incorporated the effects of organic carbon degradation on the pH of the pore water and therefore on the dissolution of $CaCO_3$, coupling organic carbon degradation and $CaCO_3$ dissolution [*Emerson and Bender,* 1981]. Because of this coupling, the steady state $[CO_3^=]$ of the ocean was very sensitive to the relative rain rates of organic carbon and $CaCO_3$ to the seafloor (the "rain ratio"). For example, a hypothetical increase in organic carbon rain rate initially lowered the global burial rate of $CaCO_3$, generating an imbalance between the incoming and outgoing fluxes of carbonate alkalinity. After a relaxation time of several thousand years, this imbalance increased $[CO_3^=]$ until burial balanced weathering again (the $CaCO_3$ compensation response).

Thus a plausible glacial increase in organic carbon production, and a decrease in calcite production, might serve as an explanation for the lower glacial pCO_2 values. Numerous sedimentological indicators suggest that the rate of productivity was generally higher in the glacial ocean than it is today [*Arrhenius,* 1988; *Lyle,* 1988; *Mix,* 1989; *Archer,* 1991b]; this is generally attributed to higher wind mixing which increases the supply rate of nutrients from subsurface waters. In today's ocean there is a general trend between production rate and organic C / $CaCO_3$ ratio measured in sediment traps (productive regions tend to organic carbon

richer sinking material) [*Honjo*, 1980; *Spencer et al.*, 1978; *Tsunogai and Noriki*, 1991]. Therefore an glacial shift in the rain ratio is not completely unexpected. This proposed degree of freedom to vary the whole ocean pH is further compelled by the recent conclusion, based on isotopes of boron, that the pH of the glacial ocean was indeed higher than present-day values [*Sanyal et al.*, 1995]. If the deep sea was more basic during glacial time, one explanation for the implied shift between the glacial lysocline and the glacial saturation depth in the water column is the rain ratio model.

To generate the entire glacial / interglacial change in atmospheric pCO_2 by a shift in whole ocean pH, the glacial decrease in atmospheric pCO_2 of a factor of one third would require an increase in deep ocean [$CO_3^=$] of about that same factor (perhaps 30 μmol kg^{-1} $CO_3^=$). The pressure effect on $CaCO_3$ solubility is approximately 20 μmol kg^{-1} km^{-1}, so that the proposed 30 μmol kg^{-1} $CO_3^=$ could drive the lysocline deeper by 1.5 km. However, while the glacial lysocline may have been offset somewhat from the present-day position [*Berger and Keir*, 1984; *Balsam and McCoy*, 1987; *Farrell and Prell*, 1989; N. Catubig, manuscript in preparation, 1995] these offsets were generally smaller than 1.5 km. Therefore the lysocline must have moved relative to $\Delta CO_3^=$; the suggestion by *Archer and Maier-Reimer* [1994] was that a change in the relative production rates of organic carbon and calcite could generate this change.

If glacial-interglacial changes in calcite and organic carbon production were responsible for a significant change in the $\Delta CO_3^=$ of the CCD between glacial time and today, as proposed by the rain ratio model, then we might expect to see the signature in today's ocean of regional variations in organic carbon / calcite production ratio. However, the 10-20 μmol kg^{-1} $CO_3^=$ variation in the depth of the CCD revealed by the data is only of order half of the 30-50 μmol kg^{-1} variation required by the rain ratio model to explain the entire atmospheric pCO_2 decrease (and only a fraction of the ~100 μmol kg^{-1} $CO_3^=$ glacial increase apparently observed by *Sanyal et al.* [1995]). The possibilities are twofold: either the rain ratio mechanism was responsible for at most half of the pCO_2 shift, or else whatever drove the glacial world calcite preservation pattern is not found within the ranges of variability for whatever factors drive calcite preservation today. This apparently rules out the relatively subtle changes in temperature between the glacial and interglacial worlds, for example. Also, it is difficult to envision glacial-interglacial changes in wind driven mixing that are larger than the regional variability in mixing in today's ocean. Iron fluxes may have been greater to the ocean during glacial time, but there are certainly areas in today's ocean where sufficient iron is available to drive production, and these areas do not exhibit the large changes in the $\Delta CO_3^=$ of the CCD required by the rain ratio model.

There is a further constraint. The lysocline in the Pacific was somewhat deeper than today, especially near the equator [*Farrell and Prell*, 1989]; the Atlantic was somewhat shallower [*Balsam and McCoy*, 1987] but relative to a scale of 1500 m the glacial-interglacial changes in the depth of the lysocline were small. Therefore if a change in whole ocean pH is responsible for the change in atmospheric pCO_2, then the lysocline must have been offset from its present position by roughly 30 μmol kg^{-1}, and it must have been so offset in a nearly uniform manner (with the possible exception of the equatorial Pacific [*Archer*, 1991b]).

Therefore we conclude that if we wish to invoke the rain ratio model as a cause of the entire glacial-interglacial pCO_2 change, we would require some globally uniform change in ocean productivity. The only possibility that comes to mind is a change in the global ocean concentration of dissolved Si. If we assume that in waters with available [Si], diatoms are able to out-compete coccoliths for the uptake of NO_3^- and PO_4^{3-}, then a change in the ratio of [Si]to [NO_3^-] and [PO_4^{3-}] in the thermocline and surface waters of the subtropical waters of the world's oceans might lead to the globally uniform change in organic carbon / calcium carbonate productivity required. The residence time of Si in the ocean is of order 15 kyr [*Treguer et al.*, 1995], and changes in ocean [Si] could have been caused either by an increase in weathering supply of Si [*Froelich et al.*, 1992] or by a change in the mechanism of removal of Si from the ocean that required higher concentrations in order for removal to balance input.

Inventory of Marine $CaCO_3$ Available for Fossil Fuel Neutralization

The irregular spacing of the ungridded $\%CaCO_3$ data set is perfectly adequate for examination of the patterns of $CaCO_3$ preservation in the ocean (previous section), but data in this format are inconvenient for calculation of global inventories and for comparison with gridded model results. Therefore a gridded field of $\%CaCO_3$ values was constructed by interpolation of the ungridded data.

$CaCO_3$ gridding method

The gridding algorithm was designed to take advantage of the well-known depth dependence of calcite concentration in deep sea sediments (the calcite lysocline). The gridded map of $\%CaCO_3$ was based on a $1^\circ \times 1^\circ$ bathymetry field (subsampled from ETOPO 5) and the regional $\%CaCO_3$ / depth relationship derived from the ungridded data. The prediction of $\%CaCO_3$ at each point in the grid is based on ungridded data points that fall within a three-dimensional ellipsoid around the target latitude, longitude, and depth. The horizontal sizes of the ellipsoids varied as a function of latitude (Figure 11) in the following way. In order to minimize spurious smoothing of any equatorial anomaly in carbonate production, equatorial sediments were isolated from sediments in the subtropical gyres by making the ellipsoids thinner near the equator; the latitudinal scale (length along the "y" major axis) of the ellipsoids ranged from $\pm 5^\circ$ on the equator to $\pm 15^\circ$ in high latitudes. Also, the longitudinal scale of the ellipsoids was $\pm 15^\circ$ at the equator and scaled up with the cosine of the latitude, to maintain a constant actual width in kilometers along the surface of the Earth. The depth scale was ± 1000 m.

Within the ellipsoid centered around the target latitude, longitude, and depth, if ungridded data existed both above and below the target depth, then the $\%CaCO_3$ for the target location was estimated using a weighted least squares regression of observed $\%CaCO_3$ as a function of depth. The ungridded data were weighted according to the horizontal and vertical distance from the target location, where the distance was scaled relative to the proportions of the ellipsoid. If the ungridded data points were all deeper or all shallower than the

Figure 11. Horizontal size distribution of the ellipsoidal regions of the influence of ungridded data onto the predicted gridded $\%CaCO_3$ field. For comparison, data locations are plotted as circles.

target bathymetry depth, then an extrapolation was performed, but only if the closest ungridded data point was within 200 m of the target bathymetry point. Finally, if the ungridded data points were all more than 400 m shallower than the target, and had less than 20% $CaCO_3$, then it was assumed that the target point contained no $CaCO_3$.

The method is able to predict each of the ungridded data points in the data set with an rms error of 15% calcite, and 13.5% calcite for data points deeper than 2000 m. This is not an exact estimate of the uncertainty in the gridded maps, since for self prediction of the input data set the error is not spatially uniformly weighted, but is rather weighted according to the density of data coverage. It appears that this rather high level of uncertainty derives from real variability in the data, and is therefore unavoidable. Figure 12 shows the rms difference in $\%CaCO_3$ between near-duplicate data points in the ungridded data set, plotted as a function of horizontal proximity. The horizontal distance was scaled to the size and aspect ratio of the ellipsoid as described above, such that a value of the scaled horizontal distance less than 1.0 means that one data point is within the ellipsoid of the other. Only data pairs for which the depths matched to within 50 m, which are deeper than 2000 m, and for which the average $\%CaCO_3$ is greater than 10%, are included in the calculation. The rms deviation of data points

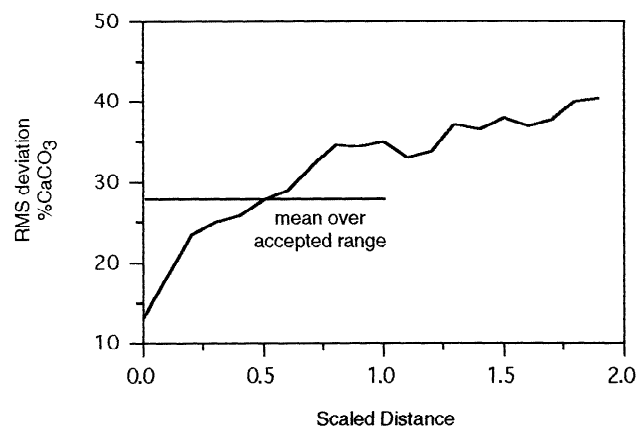

Figure 12. Root mean square difference between pairs of near-duplicate $\%CaCO_3$ measurements in the ungridded data set. Sediment depths were within 50 m. Horizontal axis is the horizontal distance between the pair, scaled to the latitudinal and longitudinal extent of the elliptical regions of influence (Figure 10). Only data for which the scaled horizontal distance was less than 1.0 were used to construct the gridded map.

from within 0.1 scaled distance units was 13%; we can consider this the best reproducibility of the measurement coupled with the natural small-scale variability of $\%CaCO_3$ in the data set. As data points diverge in space, the variability between their $\%CaCO_3$ values increases. The total rms deviation of all points within the ellipsoid distances was 27% $CaCO_3$, considerably larger than the internal predictability of the data using the depth interpolation method (13.5%). Apparently, the interpolation method is able to reduce the standard deviation of the estimate by averaging multiple data points within the ellipsoid regions.

A gridded map of $\%CaCO_3$

The resulting map of $\%CaCO_3$ in coretop sediments is presented in Figure 13. Familiar features include the high concentration of calcite in the Atlantic Ocean in response to the high pH, freshly ventilated North Atlantic Deep Water, high concentrations in the eastern equatorial Pacific, in response to high rates of calcite production and a topographic high in that region, and a sharp cutoff in calcite preservation poleward of 50° south latitude.

The map covers 80% of the ocean surface, with 56% of the missing ocean surface area in the northern hemisphere (in particular, the Arctic Ocean is a large contributor). Also, 38% of the area of missing data is shallower than 250 m in depth. The average concentration of calcium carbonate, by area weighted average and neglecting areas of missing data, is 34% dry weight. Roughly 16% of the ocean missing data area is located within the latitude range 30° S to 30° N, and at depths of less than 250 m. If we assume that half of this area is covered with 80% calcite sediment, and the rest of the areas of missing data are low calcite sediments, then the average $\%CaCO_3$ for the whole ocean surface sediment is 29%.

An inventory of erodable marine $CaCO_3$

In the coming millennia, the mechanism of $CaCO_3$ compensation will tend to neutralize much of the fossil fuel CO_2 such that the final state of the carbon will be as HCO_3^- dissolved in the oceans. The reaction to CO_2 injection will be excess $CaCO_3$ dissolution, so that neutralization can proceed by the dissolution of old $CaCO_3$ already deposited on the seafloor. Model simulations of sedimentary $CaCO_3$ dissolution indicate that dissolution is mostly confined to within the surface sediment bioturbated layer (of order 10 cm deep in the deep sea). As $CaCO_3$ is depleted from the bioturbated layer, older relict $CaCO_3$ can be entrained from below; this process is called "chemical erosion". The models indicate that dissolution (and therefore erosion) essentially stops when the bioturbated layer is filled up with nonreactive material. Thus the available inventory of $CaCO_3$ can be calculated as the extent of $CaCO_3$ dissolution necessary to fill the bioturbated layer with non-$CaCO_3$ material. A further complication is that the porosity (fractional void volume of the sediment) is observed to be higher in $CaCO_3$-poor sediments, decreasing the required mass of non-$CaCO_3$ material to fill up the bioturbated layer, and therefore decreasing the potential reach of chemical erosion.

A prediction of the porosity (ϕ) of the sediment as a function of $\%CaCO_3$ can be adapted from a dry bulk density relationship from *deMenocal et al.* [1993]:

$$\phi_{max} = 1 - \frac{0.483 + 0.0045 \times \%CaCO_3}{2.5} \quad (6)$$

where ϕ_{max} is expected porosity of sediments which are significantly below the sediment - water interface. Approaching the sediment - water interface from below, porosity increases exponentially toward the overlying water value of 1.0. I assume that the e-folding depth (α) for the low porosity surface layer varies with $\%CaCO_3$ as

$$\alpha = 0.25\text{cm} \times \frac{\%CaCO_3}{100\%} + 3.0\text{cm} \times \left(1 - \frac{\%CaCO_3}{100\%}\right) \quad (7)$$

based on results *Archer et al.* [1989] and *Jahnke et al.*, [1986]. Porosity as a function of depth is then given by

$$\phi(z) = \phi_{max} + (1 - \phi_{max})\, e^{-\frac{z}{\alpha}} \quad (8)$$

and the average porosity over the top 10 cm of the sediment column can be found by integration to be

$$\overline{\phi} = \phi_{max} - \frac{\alpha(1 - \phi_{max})}{10\text{cm}} \left(e^{-\frac{10\text{cm}}{\alpha}} - 1 \right) \quad (9)$$

where $\overline{\phi}$ is the average porosity of the mixed layer. Using $\overline{\phi}$, and a density of solid material of 2.5 g cm^{-3}, the global inventory of calcium carbonate within the 10 cm thick bioturbated layer is 6650 Gt $CaCO_3$, or ~800 Gt C. When the potential for chemical erosion is considered, the "available erosion depth", $z_{erosion}$, can be calculated as

$$z_{erosion} = 10\text{cm} \times \frac{1 - \overline{\phi}_{no\,CaCO_3}}{1 - \overline{\phi}_{with\,CaCO_3}} \left(1 - \frac{\%CaCO_3}{100\%}\right)^{-1} \quad (10)$$

where $\overline{\phi}_{with\,CaCO_3}$ and $\overline{\phi}_{no\,CaCO_3}$ is the porosity with and without $CaCO_3$. This formulation assumes that the noncalcite material in the sediments is entirely refractory, and that the $\%CaCO_3$ in the meter below the mixed layer is constant with depth. Using these assumptions, we calculate that 1600 Gt C are available for neutralization of fossil fuel CO_2. This estimate is roughly one third as large as the estimate of *Broecker and Takahashi* [1978], primarily because of the effect of the sediment porosity / $\%CaCO_3$ relationship on the potential erosion depth.

The potential deep-sea $CaCO_3$ neutralizing power may be exceeded by the eventual release of fossil fuel CO_2. *Sundquist* [1985] estimated that 5200 Gt C of coal reservoirs have been identified, and estimated that 5000-6000 Gt C of coal may ultimately be available, and that potentially available crude oil, natural gas, and oil shale inventories total roughly another 1000 Gt C. For comparison, the atmosphere contains approximately 700 Gt C. On the time scale of $CaCO_3$ compensation, weathering on land will neutralize an additional 700 Gt C (assuming continued preanthropogenic carbonate weathering rates of 1.2 Gt $CaCO_3$ yr^{-1} for 5000 years). In spite of weathering, anthropogenic emissions threaten to exceed the available neutralizing power of carbonates in the deep sea. The question is not of immediate social relevance; the timescale of fossil fuel neutralization by marine carbonates is long relative to the human timescale [*Broecker and Takahashi*, 1978]. However, the balance of fossil fuel CO_2 against the

Figure 13. Gridded map of %$CaCO_3$ in surface sediments.

reservoir of available marine carbonates will determine the long-term fate of the fossil fuel CO_2 (residence in the atmosphere versus dissolution in the ocean).

Conclusions

The distribution of sedimentary calcite in the deep sea is related to a new gridded field of water column $\Delta CO_3^=$ in an attempt to reveal regional variations in calcite preservation: the shape of the calcite lysocline. The lysocline is thicker (has a greater contrast in $\Delta CO_3^=$ between the high- and low-calcite sediments) in the western Pacific and in the Atlantic Oceans than it is in the eastern equatorial Pacific. This pattern is consistent with model response to varying rates of dilution by terriginous material. In low latitudes, calcite can be preserved to -30 μmol kg^{-1} $CO_3^=$, while calcite is depleted from higher latitude sediments by -10 μmol kg^{-1} $CO_3^=$. This gradient in calcite preservation with latitude is smaller than the glacial / interglacial shift required by the "rain ratio model" for generating lower atmospheric pCO_2 [*Archer and Maier-Reimer,* 1994], which implies that the model requires a uniform application of conditions during glacial time which have no analog in today's ocean. This conclusion rules out temperature, dust fluxes, or wind as drivers to the proposed glacial conditions, and leaves a whole ocean change in [Si] as the only possibility still remaining.

Using a gridded $\%CaCO_3$ field, we estimate that 1600 Gt of C in fossil fuel CO_2 can be neutralized by existing carbonates in the deep sea, with additional sources in shallow waters and by weathering of carbonates on land. This estimate is of order half the estimate of *Broecker and Takahashi* [1978], primarily because of the inclusion of the effect of variable sediment porosity on the potential depth of chemical erosion. The available marine $CaCO_3$ reservoir is exceeded by an estimate of the available fossil fuel reservoirs, implying that mankind has the resources to exceed the available buffering capacity of ocean $CaCO_3$.

Acknowledgments. This paper benefitted greatly from reviews by Wolf Berger and another anonymous reviewer, and discussion with Frank Richter. Printouts of the original Arrhenius sedimentary dataset were made available by Larry Mayer and Pierre Biscaye.

References

Archer, D., S. Emerson, and C. Reimers, Dissolution of calcite in deep-sea sediments: pH and O_2 microelectrode results, *Geochim. Cosmochim. Acta, 53*, 2831-2846, 1989.

Archer, D. E., Modeling the calcite lysocline, *J. Geophys. Res., 96*, 17,037-17,050, 1991a.

Archer, D. E., Equatorial Pacific calcite preservation cycles: Production or dissolution?, *Paleoceangraphy, 6*, 561-572, 1991b.

Archer, D. E., and E. Maier-Reimer, Effect of deep-sea sedimentary calcite preservation on atmospheric CO_2 concentration, *Nature, 367*, 260-264, 1994.

Arrhenius, G., Rate of production, dissolution, and accumulation of biogenic solids in the ocean, *Palaeogrogr., Palaeoclimatol., Palaeloecol., 67*, 119-146, 1988.

Balsam, W. L., and F. W. McCoy, Atlantic sediments: Glacial/interglacial comparisons, *Paleoceanography, 2*, 531-542, 1987.

Berelson, W., D. E. Hammond, J. McManus, T. E. Kilgore, M. Leinen, S. Honjo, R. Collier, and J. Dymond, Dissolution of calcium carbonate in equatorial Pacific sediments, *Eos trans. AGU,, 75(44)*, 70, 1994.

Berger, W. H., Deglacial CO_2 buildup: Constraints on the coral reef model, *Palaeogeogr. Palaeoclimatol. Palaeoecol., 40*, 235-253, 1982.

Berger, W. H., and R. S. Keir, Glacial-Holocene changes in atmospheric CO_2 and the deep-sea record, in *Climate Processes and Climate Sensitivity*, edited by J.E. Hansen and T. Takahashi, pp. 337-351, AGU, Washington, D.C., 1984.

Berger, W. H., C. G. Adelseck, and L. A. Mayer, Distribution of carbonate in surface sediments of the Pacific Ocean, *J. Geophys. Res., 81*, 2617-2627, 1976.

Biscaye, P. E., V. Kolla, and K. K. Turekian, Distribution of calcium carbonate in surface sediments of the Atlantic Ocean, *J. Geophys. Res., 81*, 2595-2603, 1976.

Boyle, E. A., Vertical oceanic nutrient fractionation and glacial/interglacial CO_2 cycles, *Nature, 331*, 55-56, 1988.

Broecker, W. S., and T. H. Peng, The role of $CaCO_3$ compensation in the glacial to interglacial atmospheric CO_2 change, *Global Biogeochem. Cycles, 1*, 15-29, 1987.

Broecker, W. S., and T. Takahashi, Neutralization of fossil fuel CO_2 by marine calcium carbonate, in *The Fate of Fossil Fuel CO_2 in the Oceans*, edited by N.R. Anderson and A. Malahof, pp. 213, Plenum, New York, 1978.

Culberson, C., and R. M. Pytkowicz, Effect of pressure on carbonic acid, boric acid, and the pH in seawater, *Limnol. Oceanogr., 13*, 403-417, 1968.

Cweink, D. S., *Recent and glacial age organic carbon and biogenic silica accumulation in marine sediments.*, masters thesis, University of Rhode Island, Narragansett,1986.

deMenocal, P. B., W. F. Ruddiman, and E. M. Pokras, Influences of high- and low-latitude processes on African terrestrial climate: Pleistocene eolian records from equatorial Atlantic Ocean Drilling Program Site 663, *Paleoceanography, 8*, 209-242, 1993.

Dickson, A. G., and F. J. Millero, A comparison of the equilibrium constants for the dissociation of carbonic acid in seawater media, *Deep Sea Res., 34*, 1733-1743, 1987.

Duce, R. A., et al., The atmospheric input of trace species to the world ocean, *Global Biogeochem. Cycles, 5*, 193-261, 1991.

Emerson, S. and D. Archer, Calcium carbonate preservation in the ocean, *Phil. Trans. R. Soc. Lond, A331*, 29-40,1990.

Emerson, S., and M. L. Bender, Carbon fluxes at the sediment-water interface of the deep sea: Calcium carbonate preservation, *J. Mar. Res., 39*, 139-162, 1981.

Emerson, S. R., and D. E. Archer, Glacial carbonate dissolution cycles and atmospheric pCO_2: A view from the ocean bottom, *Paleoceanography, 7*, 319-332, 1992.

Farrell, J. W., and W. L. Prell, Climate change and $CaCO_3$ preservation: An 800,000 year bathymetric reconstruction from the central equatorial Pacific Ocean, *Paleoceanography., 4*, 447-466, 1989.

Froelich, P. N., V. Blanc, R. A. Mortlock, S. N. Chilrud, W. Dunstan, A. Udomkit, and T.-H. Peng, River fluxes of dissolved silica to the ocean were higher during glacials: Ge/Si in diagoms, rivers, and oceans, *Paleoceanography, 7*, 739-768, 1992.

Hales, B., S. Emerson, and D. Archer, Respiration and dissolution in the sediments of the western North Atlantic: estimates from models of in situ microelectrode measurements of porewater oxygen and pH, *Deep-Sea Res., 41*, 695-719, 1993.

Honjo, S., Material fluxes and modes of sedimentation in the mesopelagic and bathypelagic aones, *J. Mar. Res., 38*, 53-97, 1980.

Jahnke, R.A., S.R. Emerson, J.K. Cochran, and D.J. Hirschberg, Fine scale distribution of porosity and particulate excess ^{210}Pb, organic carbon, and $CaCO_3$ in surface sediments of the deep equatorial Pacific. *Earth Planet. Sci. Letters, 77*, 59-69, 1986.

Keir, R. S., Dissolution of calcite in the deep sea: Theoretical prediction for the case of uniform size particles settling into a well-mixed sediment, *Am. J. Sci., 282*, 193-236, 1982.

Keir, R. S., Reconstructing the ocean carbon system variation during the last 150,000 years according to the Antarctic nutrient hypothesis, *Paleoceanography., 5*, 253-277, 1990.

Keir, R. S., and W. H. Berger, Late Holocene carbonate dissolution in the equatorial pacific: reef growth or neoglaciation?, in *The Carbon Cycle and Atmospheric CO_2: Natural Variations Archean to Present*, edited by E.T. Sundquist and W.S. Broecker, pp. 208-219, American Geophysical Union, Washington, D,C,, 1985.

Kolla, V., A. W. H. Bé, and P. Biscaye, Calcium carbonate distribution in the surface sediments of the Indian Ocean, *J Geophys. Res., 81*, 2605-2616, 1976.

Levitus, S.,*Climatological Atlas of the World Ocean*, 173 pp., U.S. Government Printing Office, Washington, D. C., 1982.

Levitus, S., M. E. Conkright, J. L. Reid, R. G. Najjar, and A. Mantyla, Distribution of nitrate, phosphate, and silicate in the world's oceans, *Prog. Ocean., 31*, 245-273, 1993.

Lyle, M., Climatically forced organic carbon burial in equatorial Atlantic and Pacific Oceans, *Nature, 335*, 529-532, 1988.

Lyman, J., *Buffer mechanism of sea water*, 196 pp., UCLA, Los Angeles, 1956.

Maier-Reimer, E., Geochemical cycles in an ocean general circulation model, Preindusrial tracer distributions, *Global Biogeochem. Cycles, 7*, 645-678, 1993.

Mehrbach, C., C. Culberson, J. E. Hawley, and R. M. Pytkowicz, Measurement of the apparent dissociation constants of carbonic acid in seawater at atmospheric pressure, *Limnol. Oceanogr., 18*, 897-907, 1973.

Mix, A. C., Influence of productivity variations on long-term atmospheric CO_2, *Nature, 337(6207)*, 541-544, 1989.

Opdyke, B. N. and J. C. G. Walker, Return of the coral reef hypothesis: Basin to shelf partitioning of $CaCO_3$ and its effect on atmospheric pCO_2, *Geology, 20*, 733-736, 1992.

Sanyal, A., G. Hemming, G. Hansen, and W. Broecker, Evidence for a higher pH in the glacial ocean from boron isotopes in foraminifera, *Nature, 373*, 234, 1995.

Sayles, F. L., The solubility of $CaCO_3$ in seawater at 2° C based upon in-situ samples pore water composition, *Mar. Chem., 9*, 223-235, 1980.

Spencer, D. W., P. G. Brewer, A. P. Fleer, S. Honjo, S. Krishnaswami, and Y. Nozaki, Chemical fluxes from a sediment trap experiment in the deep Sargasso Sea, *J. Mar. Res., 36*, 493-523, 1978.

Sundquist, E. T., Geological perspectives on carbon dioxide and the carbon cycle, in *The Carbon Cycle and Atmospheric CO_2: Natural Variations Archean to Present*, edited by E.T. Sundquist and W.S. Broecker, pp. 5, AGU, Washington D. C., 1985.

Takahashi, T., W. S. Broecker, A. E. Bainbridge, and R. F. Weiss,*Carbonate chemistry of the Atlantic, Pacific, and Indian Oceans: The results of the geosecs expeditions, 1972-1978*, Natl. Sci. Found., Washington D. C., 1980.

Treguer, P., D. M. Nelson, A. J. v. Bennekom, D. J. DeMaster, A. Leynaert, and B. Queguiner, The silica balance in the world ocean: A reestimate, *Science, 268*, 375-379, 1995.

Tsunogai, S. and S. Noriki, Particulate fluxes of carbonate and organic carbon in the ocean, Is the marine biological activity working as a sink of the atmospheric carbon?, *Tellus, 43B*, 256-266, 1991.

D.E. Archer, Department of the Geophysical Sciences, 5734 South Ellis Avenue, University of Chicago, Chicago, IL 60637.
(email: darcher@uchicago.edu)

(Received December 13, 1994; revised August 14, 1995; accepted September 18, 1995.)